Sensors and Materials, Vol. 35, No. 12 (2023) 4029–4047
MYU Tokyo

S & M 3466

Convolutional Fuzzy Neural Predictor for Blood Pressure Estimation from Electrocardiography and Photoplethysmography Signals

Cheng-Jian Lin,[1*] Mei-Yu Wu,[2] Chun-Jung Lin,[1] and Shih-Lung Shen[1]

[1]Department of Computer Science & Information Engineering, National Chin-Yi University of Technology, Taichung 411, Taiwan
[2]Department of Business Management, National Taichung University of Science and Technology, Taichung 404, Taiwan

(Received July 14, 2023; accepted November 14, 2023)

Keywords: blood pressure (BP) prediction, electrocardiography (ECG), feature fusion, fuzzy neural network (FNN), photoplethysmography (PPG), Shapley additive explanations (SHAP)

Hypertension is a major risk factor for cardiovascular disease, coronary heart disease, stroke, and other diseases. According to statistics from the World Health Organization, the number of deaths caused by cardiovascular disease is as high as 17 million each year. In this study, a convolutional fuzzy neural predictor (CFNP) model was developed to estimate systolic blood pressure (SBP), diastolic blood pressure (DBP), and mean arterial pressure (MAP). The developed CFNP model uses a convolutional layer to extract features from photoplethysmography and electrocardiography sensing signals. It then uses a maximum pooling layer to compress these features to reduce the number of calculations. A feature fusion layer is added to the developed model to integrate information from the convolutional layer and reduce the input dimension of the fuzzy neural network (FNN). Finally, the fused feature information is sent to the FNN for prediction. The Shapley additive explanations (SHAP) method was used in this study to perform feature analysis and calculate the contribution of each extracted feature. On the basis of the aforementioned analysis and calculations, superior feature sets were selected for the developed model. Experimental results indicated that the mean absolute errors (MAEs) of the CFNP model in predicting MAP, SBP, and DBP when using the superior feature sets obtained through SHAP analysis were 9.34, 14.13, and 9.39 mmHg, respectively. The proposed model also outperformed other machine learning models in terms of MAE in MAP, SBP, and DBP predictions.

1. Introduction

Human beings live in a society with plenty of food and clothing, but diseases of modern civilization quietly appear in our lives, such as high blood pressure, diabetes, and cardiovascular disease. Today, clinicians routinely diagnose and classify diseases on the basis of signal

*Corresponding author: e-mail: cjlin@ncut.edu.tw
https://doi.org/10.18494/SAM4584

ISSN 0914-4935

information collected from physiological sensors. Biomedical sensing signals, if processed correctly and efficiently, have the potential to facilitate advanced monitoring, diagnosis, and treatment planning.[1] Biomedical sensors use semiconductor technology to measure human physiological parameters in a continuous, real-time, and noninvasive manner.[2] Electrocardiography (ECG)-,[3] electromyography (EMG)-,[4] and electroencephalography (EEG)-[5] based sensors merge the fields of microelectromechanics, biology, and chemistry. The development of electrochemical sensors is particularly promising owing to their low cost, simplicity, and portability.[6]

Blood pressure (BP) is often expressed in terms of systolic BP (SBP) (i.e., the pressure within the blood vessels when the heart contracts) and diastolic BP (DBP) (i.e., the pressure within the blood vessels when the heart relaxes). Under normal circumstances, the BP of a healthy person is below 120/80 mmHg. If the BP is between 120/80 and 140/90 mmHg, prehypertension occurs, and when the BP exceeds 140/90 mmHg,[7] hypertension occurs. Hypertension is a major risk factor for cardiovascular disease, coronary heart disease, stroke, and other diseases. According to statistics from the World Health Organization,[8] the number of deaths caused by cardiovascular disease is as high as 17.3 million per year. Of these deaths,[8] 7.3 million are caused by coronary heart disease and 6.2 million are caused by stroke. Because prehypertension usually has no obvious symptoms and most people do not measure their BP regularly, they do not know that they have high BP until their vital organs are damaged. Therefore, the regular monitoring of BP is crucial for the early diagnosis of hypertension. Currently, the standard sphygmomanometers[9] used in clinical practice are the mercury sphygmomanometer and electronic sphygmomanometer.

Because the aforementioned two devices can be used for the intermittent measurement of BP, many researchers[10–13] have attempted to develop noninvasive cuffless BP measurement technology. Most noninvasive cuffless BP measurement methods involve extracting features from electrocardiography (ECG) or photoplethysmography (PPG) signals and using these features to estimate BP. Poon and Zhang[10] developed a cuffless and noninvasive technique for BP prediction. This technique involves predicting BP by using the time interval from the R wave of an ECG signal to the feature point of a PPG signal at a predetermined threshold in the same heartbeat cycle. This time interval is called pulse transit time (PTT). The cuffless BP measurement technology proposed in Ref. 10 can meet the standards required for medical diagnosis and can be used in wearable devices. If the PTT is insufficiently long for tracking the low-frequency (LF) oscillation of arterial BP (ABP), the accuracy of BP prediction is unsatisfactory. To overcome this problem, Ding *et al.*[11] proposed a new feature called photoplethysmogram intensity ratio (PIR). This feature can be used to track LF oscillations of changes in BP caused by changes in arterial diameter. The aforementioned authors developed a BP prediction model based on PIR and PTT, and this model was more accurate than the model based on only PTT. Thambiraj *et al.*[12] proposed an algorithm that takes the PTT, PIR, and Womersley number (α) as inputs to achieve continuous cuffless BP monitoring. The Womersley number of the viscous effect influences BP, and the results in Ref. 12 indicated that a high accuracy was achieved when α was used to predict BP. Cattivelli and Garudadri[13] proposed a method for predicting BP on the basis of pulse arrival time (PAT) and heart rate (HR). PAT

represents the delay between the Q-, R-, and S-wave (QRS) peak of an ECG signal and the corresponding point of a PPG signal. HR and PAT are used to achieve high robustness in measurements of random deviation. Therefore, these parameters were the input features of the model developed in this study.

Continuous and noninvasive BP prediction has not been fully realized in previous studies. With the rapid development of artificial intelligence, machine learning methods have been introduced into medicine, including those for noninvasive BP prediction. For example, Zhang *et al.*[14] proposed a classification and regression tree model based on features such as ECG signals, PPG signals, PTT, oxygen saturation (SPO_2), and HR for BP prediction. This model uses a cross-validation method for automatically determining and optimizing the aforementioned parameters. The results described in Ref. 16 indicated that the prediction accuracy of the aforementioned model was more than 90%, with an error range of ±5 mmHg. Hsieh *et al.*[15] proposed a linear regression model for predicting SBP and DBP. This model combines static and dynamic PTT features to achieve a high correlation coefficient (R^2) and a low mean squared error (MSE). However, finding features related to BP for machine-learning-based BP prediction models requires considerable time and relevant knowledge. Therefore, some studies have used deep learning methods for BP prediction. Lee and Chang[16] proposed a regression model based on a deep belief network, which is a type of deep neural network, and artificial features obtained through bootstrap technology to predict SBP and DBP.[17] This model outperformed traditional algorithms and achieved an overall grade of A in terms of the British Hypertension Society score. Pan *et al.*[18] developed an automatic BP measurement method based on deep learning. A convolutional neural network (CNN) was used to identify Korotkoff sounds, which are heard with a stethoscope during noninvasive BP measurement. The results described in Ref. 18 indicated that the aforementioned method is effective and can be used as an alternative to oscillometry-based automatic BP measurement.

CNNs are currently the most commonly used deep learning networks, and they consist of convolutional layers, pooling layers, flat layers, and fully connected layers. Compared with traditional machine learning algorithms, CNNs can more effectively automatically extract crucial features and identify rules from them. However, the fully connected layers used in a CNN increase its number of parameters, hardware requirements, and computing time. Therefore, some researchers have used fuzzy neural networks (FNNs) to reduce the number of model parameters. Fuzzy logic is a multivalued logic that takes infinite values in the interval [0, 1]. In fuzzy logic, a membership function is used to represent the degree to which an element belongs to a fuzzy set. Fuzzy logic resembles human thinking and can be used to solve complex problems easily by using expert knowledge. FNNs[19] are frequently used in medical diagnosis. Jang[20] proposed an adaptive neurofuzzy inference system, using a hybrid algorithm to improve the accuracy of diabetes classification for increasing the accuracy of predicting patients with cardiovascular disease. Terrada *et al.*[21] used fuzzy logic to establish a fuzzy expert system for the diagnosis of heart disease. Le[22] proposed a fuzzy C-means clustering interval type-2 cerebellar model articulation neural network to improve the diagnostic accuracy of breast cancer and liver disease.

In this study, a convolutional fuzzy neural predictor (CFNP) model was developed for the noninvasive continuous prediction of SBP, DBP, and mean arterial pressure (MAP). The input of

this model comprises features extracted from denoised PPG and ECG signals. The developed CFNP comprises a convolutional layer, a feature fusion layer, and an FNN layer. The feature fusion layer is used to integrate information from the convolutional layer and reduce the input dimension of the FNN. To reduce the number of adjustable parameters, an FNN is used instead of a fully connected neural network. The Shapley additive explanations (SHAP) method is used to analyze the contribution of each feature for conducting dimensionality reduction. In summary, the major contributions of this study are as follows.

(1) A CFNP model is proposed for the prediction of SBP, DBP, and MAP based on the features extracted from PPG and ECG signals.
(2) Four fusion methods, namely, global max pooling (GMP), global average pooling (GAP), channel max pooling (CMP), and channel average pooling (CAP), are used in the proposed model to integrate information from its convolutional layer. These fusion methods reduce the input dimension and shorten the operation time of the predictor network.
(3) An FNN is used instead of a fully connected neural network in the proposed CFNP model to reduce the number of parameters to be adjusted in this model.
(4) The SHAP method is used to analyze the contribution of each feature extracted from PPG and ECG signals to establish a CFNP model with low-dimensional feature input.

The rest of this paper is organized as follows. Section 2 provides a detailed introduction of the overall architecture of the developed model. Section 3 presents the experimental results obtained using the developed CFNP model and other models. Section 4 concludes the study and provides recommendations for future research.

2. Materials and Methods

Figure 1 shows the architecture of the proposed model for cuffless BP prediction. The steps involved in the proposed model are described in the following text. First, PPG and ECG signals are preprocessed and features are extracted. Second, the extracted features are used as the input signal of the CFNP model. Third, the one-dimensional (1D) convolutional layer in the CFNP is used to extract features of the input data. Fourth, fusion methods are used to reduce the number of model parameters. Fifth, the features obtained from the fusion layer are used as the input of the FNN. Sixth, the FNN outputs the predicted SBP, DBP, and MAP. These steps are detailed in the following subsections.

2.1 Preprocessing and feature extraction

The signal preprocessing method in Ref. 23 was used in this study. The third-order Butterworth bandpass finite impulse response filter was used to remove artifacts from the collected signals. The 23 features used in Refs. 23 and 24 were used as the input of the proposed model. The definitions of these features are presented in Table 1.

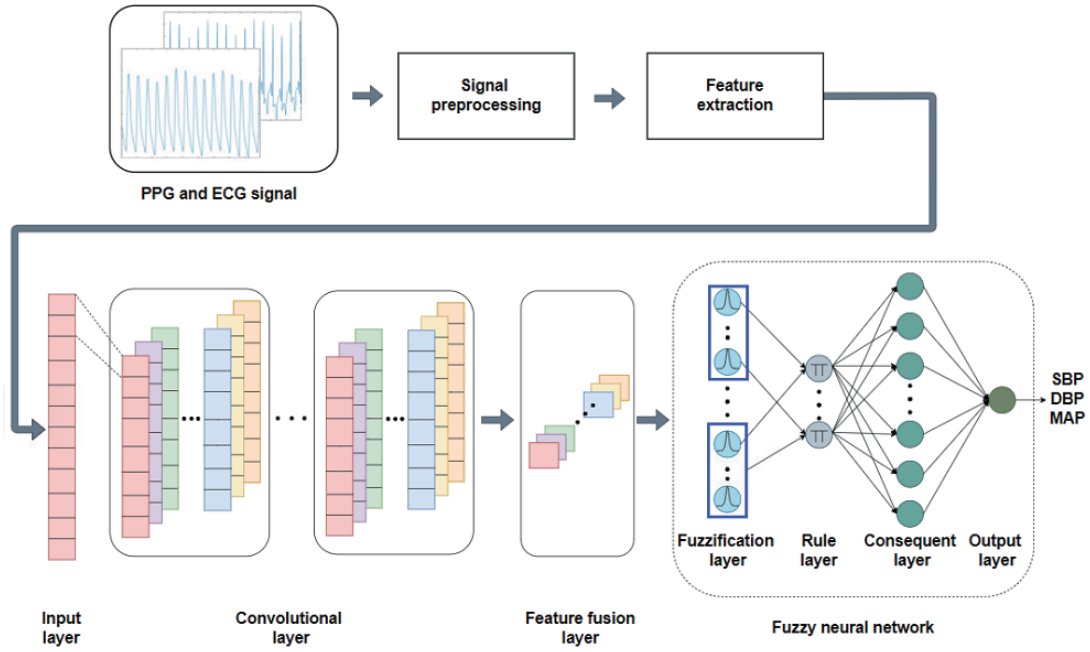

Fig. 1. (Color online) Architecture of the proposed model for cuffless BP prediction.

Table 1
Detailed definitions of the features used in Refs. 23 and 24.

Feature Name	Definition	Feature Name	Definition
alpha	Womersley number	SW25	Systolic Width at 25%
hrfinal	Heart rate	SW25+DW25	Systolic Width at 25% + Diastolic Width at 25%
ih	Highest intensity of PPG	DW25/SW25	Diastolic Width at 25% / Systolic Width at 25%
il	Lowest intensity of PPG	SW33	Systolic Width at 33%
meu	AC component max amplitude of PPG	SW33+DW33	Systolic Width at 33% + Diastolic Width at 33%
PIR	Photoplethysmogram intensity ratio	DW33/SW33	Diastolic Width at 33% / Systolic Width at 33%
PTT	Pulse transmission time	SW50	Systolic Width at 50%
SUT	Systolic upstroke time	SW50+DW50	Systolic Width at 50% + Diastolic Width at 50%
DT	Diastolic time	DW50/SW50	Diastolic Width at 50% / Systolic Width at 50%
SW10	Systolic width at 10%	SW66+DW66	Systolic Width at 66% + Diastolic Width at 66%
SW10+DW10	Systolic width at 10% + Diastolic width at 10%	SW75+DW75	Systolic Width at 75% + Diastolic Width at 75%
DW10/SW10	Diastolic width at 10% / Systolic width at 10%		

2.2 Proposed CFNP

The proposed CFNP has a three-layer network architecture. It comprises a convolutional layer, a feature fusion layer, and an FNN layer. Each layer is described in detail as follows.

2.2.1 Convolutional layer

The features extracted from PPG and ECG signals are used as the input of the convolutional layer, and a feature map is obtained through the convolution operation by using a convolutional kernel with a sliding window. The output formula for the convolution operation is

$$O_{fm}(fn) = \sum_{n=0}^{Xs} I(n) \times X_w(n, fn), \tag{1}$$

where O_{fm} is the output feature map, fn is the number of output feature maps, I is the input of the convolutional layer, X_w is the weight of the convolutional kernel, and Xs is the size of the convolutional kernel.

2.2.2 Feature fusion layer

The feature fusion layer uses four fusion methods, namely, GAP [Fig. 2(a)], GMP [Fig. 2(a)], CAP [Fig. 2(b)], and CMP [Fig. 2(b)], to integrate information from the convolutional layer of the proposed CFNP. These fusion methods reduce the input dimension of the predictor and shorten its operation time. The aforementioned methods and their formulas are described as follows.

(1) GAP

GAP involves the calculation of the average value of each feature map output using the convolutional layer; that is, the average value of each feature map is the output.

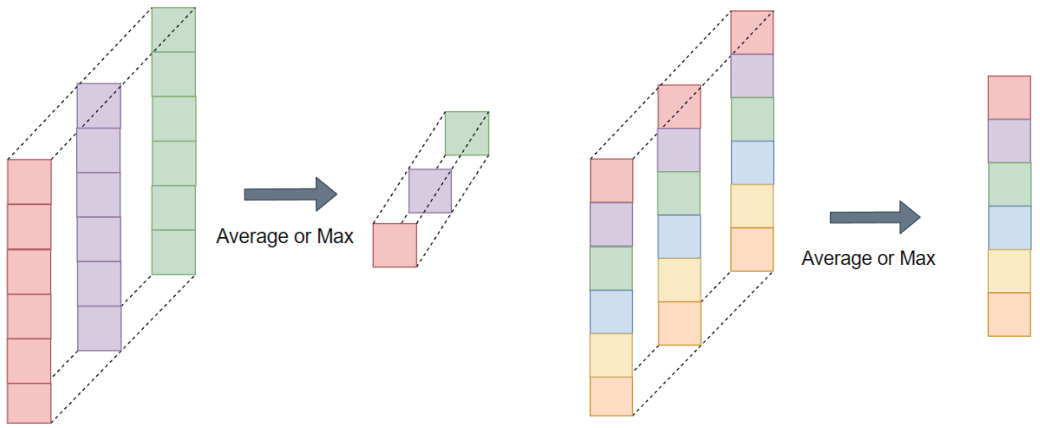

Fig. 2. (Color online) Feature fusion methods: (a) global pooling and (b) channel pooling.

$$O_{GAP}(g) = Avg\left(I_{fm}(fn)\right) \tag{2}$$

Here, O_{GAP} is the output of the feature fusion layer when conducting GAP, I_{fm} is the input feature map, g is the output size of the fusion layer, and fn is the number of feature maps.

(2) GMP

GMP involves the calculation of the maximum value of each feature map output by the convolutional layer; that is, the maximum value of each feature map is the output.

$$O_{GMP}(g) = Max\left(I_{fm}(fn)\right) \tag{3}$$

Here, O_{MGP} is the output of the feature fusion layer when conducting GMP, I_{fm} is the input feature map, g is the output size of the fusion layer, and fn is the number of feature maps.

(3) CAP

CAP involves the calculation of the average value of each channel for the feature map output by the convolutional layer; that is, the average value of each channel is the output.

$$O_{CAP}(c) = Avg\left(I_{fm}(fn)\right) \tag{4}$$

Here, O_{CAP} is the output of the feature fusion layer when conducting CAP, I_{fm} is the input feature map, c is the output size of the fusion layer, and fn is the number of feature maps.

(4) CMP

CMP involves the calculation of the maximum value of each channel for the feature map output by the convolutional layer; that is, the maximum value of each channel is the output.

$$O_{CMP}(c) = Avg\left(I_{fm}(fn)\right) \tag{5}$$

Here, O_{CMP} is the output of the feature fusion layer when performing CMP, I_{fm} is the input feature map, c is the output size of the fusion layer, and fn is the number of feature maps.

2.2.3 FNN

The FNN of the proposed model comprises a fuzzification layer, a rule layer, a consequent layer, and an output layer.

(1) Fuzzification Layer

First, the FNN performs a fuzzification operation on the feature map output by the feature fusion layer. Each node represents a fuzzy set in the interval [0, 1]. The triangular, trapezoidal, and Gaussian membership functions are commonly used. The application of differentiable membership functions to FNNs has advantages. Gaussian membership functions are popular as membership functions for FNNs.[25] Therefore, a Gaussian function is used in the proposed model, and an if–then fuzzy rule is used for fuzzy inference. The adopted Gaussian membership function is expressed as

$$O_f(i,j) = \exp\left(-\frac{\left(I_{fusion}(i) - M(i,j)\right)^2}{\left(SD(i,j)\right)^2} \right), \tag{6}$$

where O_{CMP} is the output of the feature fusion layer when performing CMP, I_{fm} is the input feature map, c is the output size of the fusion layer, and fn is the number of feature maps.

(2) Rule Layer

The rule layer determines the excitation intensity of each rule through the product operation for each node obtained in the previous layer. This operation is expressed as

$$O_r(j) = \prod_{i=1}^{n} I_f(i,j), \tag{7}$$

where $O_r(j)$ is the output of the rule layer, $I_f(i, j)$ is the degree of excitation of each node, and n is the number of input nodes.

(3) Consequent Layer

The consequent layer uses the mean value of the Gaussian membership function as the weight value. The relevant formula is

$$O_c(i) = W_c(i), \tag{8}$$

where $O_r(j)$ is the output of the rule layer, $I_f(i, j)$ is the degree of excitation of each node, and n is the number of input nodes.

(4) Output Layer

Finally, the output of the rule layer is multiplied by the weight of the consequent layer to obtain MAP, SBP, and DBP predictions. The relevant formula is

$$O = \sum_{i=1}^{k} I_c(i) W_c(i), \tag{9}$$

where $I_c(i)$ is the output of the rule layer and $W_c(i)$ is the weight of the consequent layer.

3. Experimental Results

In this section, the data source, namely, the Multiparameter Intelligent Monitoring in Intensive Care (MIMIC) II waveform database, is introduced. The proposed model was compared with its machine learning counterparts in terms of accuracy in predicting MAP, SBP, and DBP. The reduced-dimensionality feature set obtained through SHAP analysis was used to verify the results of each BP prediction model.

3.1 Data set

The MIMIC II waveform data set was used in this study.[26] This data set contains data on three types of signal, namely, ECG signals obtained in bipolar limb lead configuration II, PPG signals, and ABP measured using an invasive method. The PPG, ECG, and ABP signals are shown in Fig. 3. The aforementioned data set contains 12000 data points, and the sampling frequency of each signal is 125 Hz. In the experiments conducted in this study, ABP signals

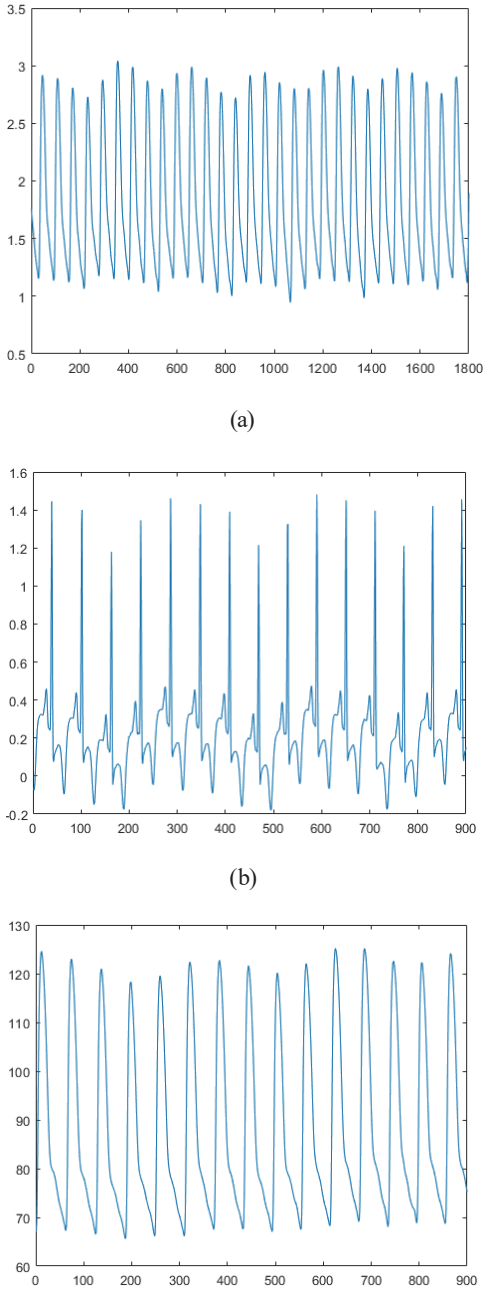

Fig. 3. (Color online) (a) PPG, (b) ECG, and (c) ABP signals.

were used to obtain SBP and DBP, and the MAP was then calculated from the predicted values of SBP and DBP. Furthermore, SBP values of ≥180 and ≤80 and DBP values of ≥130 and ≤60 were filtered out. Finally, a total of 4631 data points remained in the data set for the experiment. Figure 4 and Table 2 present the descriptive statistics for MAP, SBP, and DBP. In the experiments, 80, 10, and 10% of the data set's data were used as training, validation, and testing data, respectively.

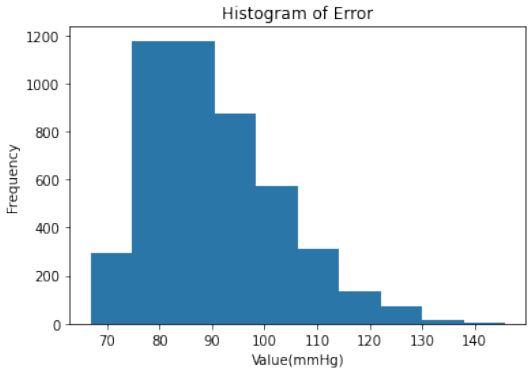

(a)

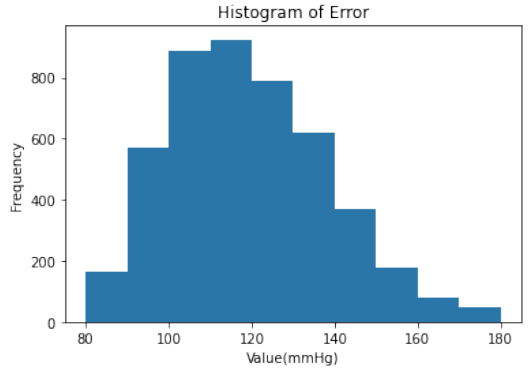

(b)

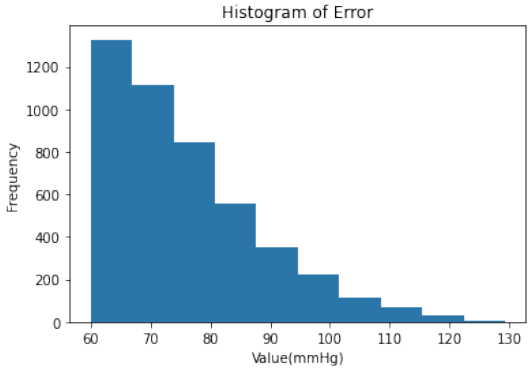

(c)

Fig. 4. (Color online) Data distribution range for (a) MAP, (b) SBP, and (c) DBP.

Table 2
Statistics related to MAP, SBP, and DBP.

	Max (mmHg)	Min (mmHg)	Mean (mmHg)	STD (mmHg)
MAP	145.83	66.81	12.43	90.4
SBP	179.98	80.09	18.89	119.34
DBP	129.25	60.03	12.61	75.93

3.2 Experimental results obtained using the proposed CFNP model

The 23 features presented in Table 1 were input into the proposed model to predict MAP, SBP, and DBP. Table 3 presents the mean absolute errors (MAEs) and root MSEs (RMSEs) obtained for MAP, SBP, and DBP when the four fusion methods adopted in this study were used. As presented in Table 3, the best prediction results for MAP, SBP, and DBP were obtained when GMP, CAP, and CMP were used, respectively. Therefore, in the following experiments, GMP, CAP, and CMP were used to predict MAP, SBP, and DBP, respectively.

Tables 4–6 describe the architectures of the proposed CFNP when GMP, CAP, and CMP are used to predict MAP, SBP, and DBP, respectively. These architectures contain eight layers, including three 1D convolutional layers, one feature fusion layer, and one FNN layer.

3.3 Dimension reduction through SHAP analysis

The architectures used to predict MAP, SBP, and DBP were analyzed using the SHAP method.[27] SHAP is an additive explanatory model based on the Shapley value. The Shapley value is a solution proposed by Lloyd Stowell Shapley[28] on the basis of cooperative game theory. In this study, the SHAP method was used to analyze the contribution of each factor in the architectures used for the predictions of MAP, SBP, and DBP; that is, the Shapley value of each feature was calculated to evaluate its contribution to the prediction. Figures 5–7 depict the results of the SHAP analysis for MAP, SBP, and DBP predictions, respectively. Figures 5(a), 6(a), and 7(a) represent visualizations of Shapley values. In these figures, the horizontal axis represents the SHAP value, each row represents a feature, and each point represents a sample. A higher red intensity in Figs. 5(a), 6(a), and 7(a) indicates a higher Shapley value of a feature. By contrast, the higher the blue intensity in these figures, the lower the Shapley value of a feature. As shown in Figs. 5(b), 6(b), and 7(b), the mean absolute value of the degree of influence of each feature on the target variable was used as the importance index of the feature. Thus, the higher the blue intensity of a feature, the higher its degree of influence on the prediction.

As depicted in Fig. 5(b), il (i.e., lowest intensity of the PPG signal) was the most important feature affecting MAP prediction, followed by SW10 + DW10 (i.e., systolic width at 10% + diastolic width at 10%) and SW10 (i.e., systolic width at 10%). As shown in Fig. 6(b), the average Shapley values of meu and DW10/SW10, which were the 12th and 13th most important features affecting SBP, respectively, considerably differed. Therefore, the 12 most important features were used as a new feature set. Table 7 presents the 12 most important features identified through SHAP analysis for MAP, SBP, and DBP predictions. The remaining features were filtered out. Thus, dimensionality reduction was achieved to reduce the training time of the CFNP model.

Table 3
MAP, SBP, and DBP predicted using the proposed CFNP model with the 23 features presented in Table 1.

Method	Feature fusion	MAP		SBP		DBP	
		MAE	RMSE	MAE	RMSE	MAE	RMSE
CFNP	CAP	9.42	12.03	14.26	17.87	9.52	12.06
	CMP	9.48	12.09	14.32	18.25	9.46	11.93
	GAP	9.54	12.16	14.54	18.25	9.53	11.94
	GMP	9.40	12.00	14.57	18.27	9.55	12.20

Table 4
Architecture of the proposed CFNP when using GMP for MAP prediction.

Layer	Filter	Kernel	Layer Parameters
Input Layer	—	—	—
Convolution Layer1	64	3	Strides = 1,ReLU
Convolution Layer2	32	2	Strides = 1,ReLU
Convolution Layer3	16	2	Strides = 1,ReLU
Global Max Pooling Layer	—	—	—
Fuzzy Rule Layer	—	—	Rule = 32
Consequent Layer	16	1	ReLU
Output Layer	1	1	—

Table 5
Architecture of the proposed CFNP when using CAP for SBP prediction.

Layer	Filter	Kernel	Layer Parameters
Input Layer	—	—	—
Convolution Layer1	64	3	Strides = 1,ReLU
Convolution Layer2	32	2	Strides = 1,ReLU
Convolution Layer3	16	2	Strides = 1,ReLU
Channel Average Pooling Layer	—	—	—
Fuzzy Rule Layer	—	—	Rule = 64
Consequent Layer	16	1	ReLU
Output Layer	1	1	—

Table 6
Architecture of the proposed CFNP when using CMP for DBP prediction.

Layer	Filter	Kernel	Layer Parameters
Input Layer	—	—	—
Convolution Layer1	64	3	Strides = 1,ReLU
Convolution Layer2	32	2	Strides = 1,ReLU
Convolution Layer3	16	2	Strides = 1,ReLU
Channel Max Pooling Layer	—	—	—
Fuzzy Rule Layer	—	—	Rule = 64
Consequent Layer	16	1	ReLU
Output Layer	1	1	—

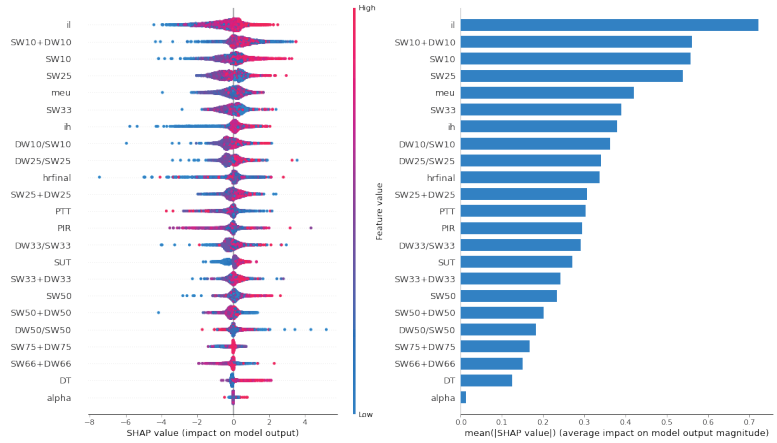

(a) (b)

Fig. 5. (Color online) (a) Shapley values and (b) average Shapley values for MAP prediction.

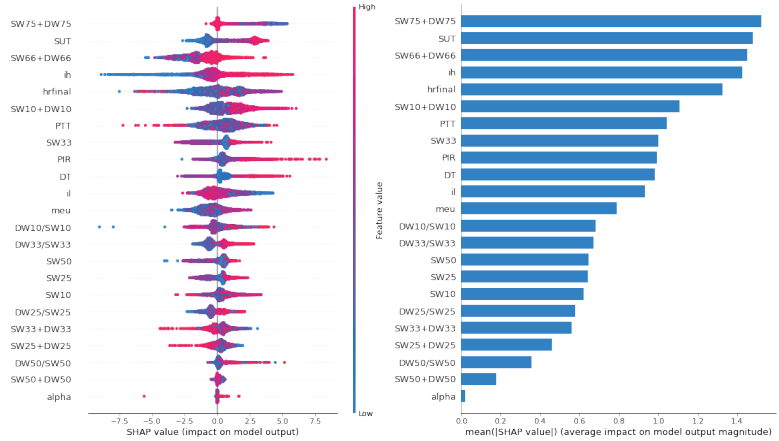

(a) (b)

Fig. 6. (Color online) (a) Shapley values and (b) average Shapley values for SBP prediction.

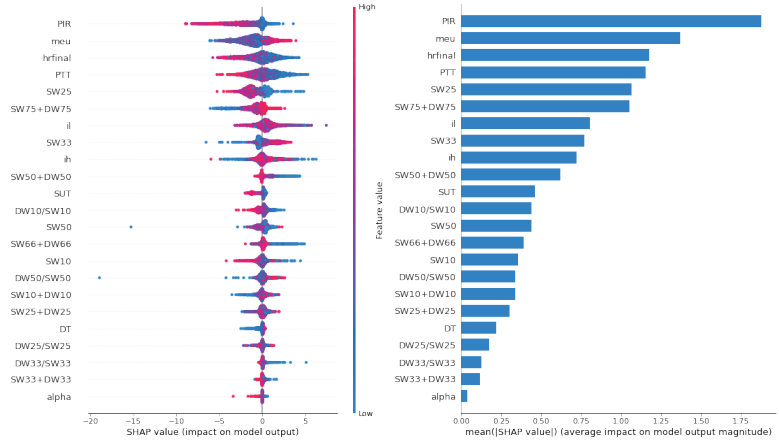

(a) (b)

Fig. 7. (Color online) (a) Shapley values and (b) average Shapley values for DBP prediction.

Table 7
New feature sets (covering the 12 most important features) obtained for MAP, SBP, and DBP predictions through SHAP analysis.

MAP	SBP	DBP
il	SW75+DW75	PIR
ST10+DT10	SUT	meu
SW10	SW66+DW66	hrfinal
SW25	ih	PTT
meu	hrfinal	SW25
SW33	SW10+DW10	SW75+DW75
ih	PTT	il
DW10/SW10	SW33	SW33
DW25/SW25	PIR	ih
hrfinal	DT	SW50+DW50
DW25+SW25	il	SUT
PTT	meu	DW10/SW10

By using the new feature sets presented in Table 7, the CFNP model used for MAP, SBP, and DBP predictions was retrained. Table 8 presents the experimental results obtained when using the new feature sets. As presented in Table 8, the MAEs of the MAP, SBP, and DBP predictions decreased from 9.40, 14.26, and 9.46 to 9.34, 14.13, and 9.39, respectively.

In addition, MAP, SBP, and DBP predictions were output from a general CNN model.[29] A CNN includes convolutional layers and fully connected layers. In contrast to the proposed CFNP, which contains an FNN, CNNs contain a fully connected layer. In this study, the number of parameters of the CNN model was 13745, and the numbers of parameters of the CFNP model for MAP, SBP, and DBP predictions were 6993, 7505, and 7505, respectively. Thus, the CFNP model had approximately 6000 fewer parameters than the CNN model.

Figures 8(a)–8(c) display the prediction error histograms for the MAP, SBP, and DBP predicted using the CFNP model, respectively. Because SBP had a wider data range than MAP and DBP, the error range of SBP prediction was 30–35 mmHg larger than those of MAP and DBP predictions.

Figure 9 presents the Bland–Altman plots for the MAP, SBP, and DBP predictions obtained using the CFNP model, respectively. As depicted in Fig. 9, the prediction errors of MAP and DBP were within ±20 mmHg, and the prediction error of SBP was within ±40 mmHg. However, for very high and very low BP values, considerable differences existed in the prediction accuracy of the CFNP model because limited samples with such values are limited in the adopted data set; therefore, poor prediction results were obtained for the aforementioned BP values.

3.4 Comparison of the results obtained using different models

The results obtained with the proposed CFNP model were compared with those of four other prediction models, namely, the K-nearest neighbors (KNN),[30] support vector regression (SVR), [31] linear regression,[32] and CNN[33]models. Table 9 presents the BP prediction results obtained using the aforementioned models. The results presented in Table 9 indicate that the proposed CFNP model had smaller MAE and RMSE values than the KNN,[30] SVR,[31] linear regression,[32] and CNN[33] models in predictions of MAP, SBP, and DBP.

Table 8
Experimental results obtained using the 12 most important features.

BP predict	Method	Parameters	Regression indicator	
			MAE	RMSE
MAP	CFNP with GMP	6993	9.34	12.00
SBP	CFNP with CAP	7505	14.13	17.97
DBP	CFNP with CMP	7505	9.39	12.04

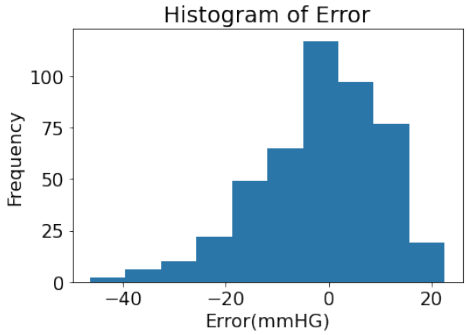

(a)

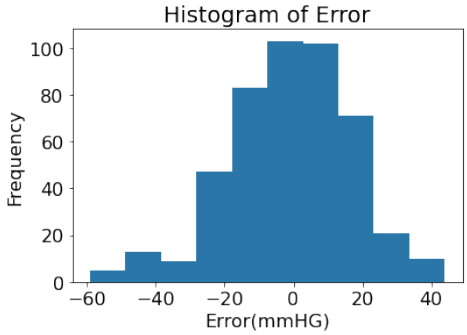

(b)

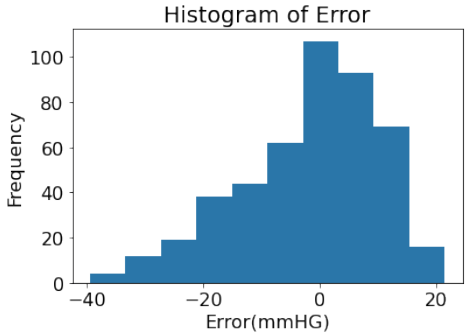

(c)

Fig. 8. (Color online) Prediction error histograms of (a) MAP, (b) SBP, and (c) DBP obtained using the CFNP model.

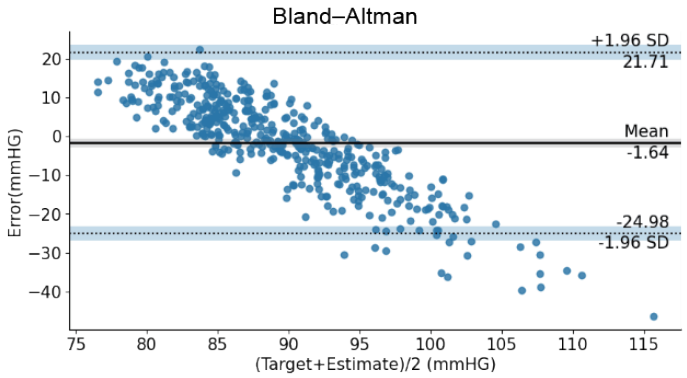

(a)

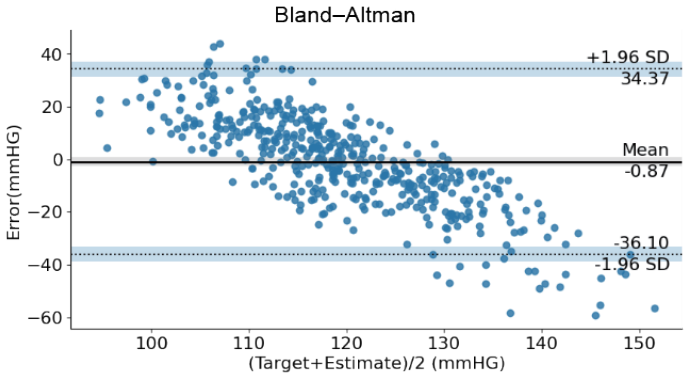

(b)

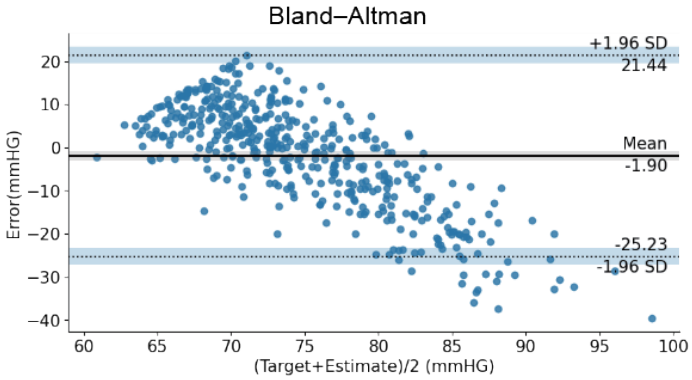

(c)

Fig. 9. (Color online) Bland–Altman plots of (a) MAP, (b) SBP, and (c) DBP predictions obtained using the CFNP model.

Table 9
Comparison of the results obtained using different models.

Method	Feature fusion	MAP		SBP		DBP	
		MAE	RMSE	MAE	RMSE	MAE	RMSE
KNN[30]	—	9.93	12.69	15.13	19.33	10.22	12.76
Linear regression[32]	—	9.62	11.92	14.76	18.38	9.79	11.90
SVR[31]	—	9.46	12.55	14.71	18.90	9.47	12.54
CNN[33]	—	9.42	12.06	14.52	18.26	9.44	12.10
Proposed CFNP	GMP	9.34	12.00	—	—	—	—
	CAP	—	—	14.13	17.97	—	—
	CMP	—	—	—	—	9.39	12.04

4. Conclusion

In this study, a CFNP model was developed for the noninvasive continuous predictions of SBP, DBP, and MAP from sensing signals. The proposed CFNP comprises a convolutional layer, a feature fusion layer, and an FNN layer. The feature fusion layer is used to integrate information from the convolutional layer and reduce the dimensionality of the input of the FNN. An FNN is used instead of a fully neural network to reduce the number of adjustable model parameters. The SHAP method was used to analyze the contribution of each feature to the prediction for conducting dimensionality reduction. In addition, Bland–Altman plots of MAP, SBP, and DBP predicted using the proposed CFNP were analyzed. Experimental results indicated that the MAEs of the CFNP model in MAP, SBP, and DBP predictions when using the superior feature sets obtained through SHAP analysis were 9.34, 14.13, and 9.39 mmHg, respectively. Moreover, the proposed CFNP model had smaller MAE and RMSE values than the KNN, SVR, linear regression, and CNN models in MAP, SBP, and DBP predictions.

In future studies, the proposed CFNP can be implemented in hardware devices, such as field programmable gate arrays (FPGAs), for real-time applications. The parameters of each layer of the proposed CFNP can be translated into FPGAs in the future for verification to pave the way for hardware implementation.

Acknowledgments

Funding: This research was funded by the National Science and Technology Council of the Republic of China, grant number NSTC 112-2221-E-167-026.

Conflicts of Interest: The authors declare no conflicts of interest regarding the publication of this paper.

References

1 S. Begum, S. Barua, and M. U. Ahmed: Sensors **14** (2014) 11770. https://doi.org/10.3390/s140711770
2 X. Li, J. Dunn, D. Salins, G. Zhou, W. Zhou, S. M. S. Rose, D. Perelman, E. Colbert, R. Runge, S. Rego, R. Sonecha, S. Datta,T. McLaughlin, and M. P. Snyder: PLOS Biol. **15** (2017) e2001402. https://doi.org/10.1371/journal.pbio.2001402

3 A. J. Bandodkar and J. Wang: Trends Biotechnol. **32** (2014) 363. https://doi.org/10.1016/j.tibtech.2014.04.005
4 J. Taelman, T. Adriaensen, C. Horst, T. Linz, and A. Spaepen: Proc. 2007 29th Annu. Int Conf. IEEE Engineering in Medicine and Biology Society (2007) 3966–3969. https://doi.org/10.1109/IEMBS.2007.4353202
5 J. L. Park, M. M. Fairweather, and D. I. Donaldson: Neurosci. Biobehav. Rev. **52** (2015) 117. https://doi.org/10.1016/j.neubiorev.2015.02.014
6 R. A. S. Couto and M. B. Quinaz: Sensors **16** (2016) 1. https://doi.org/10.3390/s16071015
7 F. D. Fuchs and P. K. Whelton: J. Hypertens. **75** (2020) 2. https://doi.org/10.1161/HYPERTENSIONAHA.119.14240
8 S. Mendis, P. Puska, and B. Norrving: World Health Organization (2011) https://apps.who.int/iris/handle/10665/44701 (accessed June 2022).
9 Y. Ostchega, G. Zhang, P Sorlie, J. P. Hughes, D. S. Reed-Gillette, T. Nwankwo, and S. Yoon: Natl. Health Stat. Report **59** (2012) 1. https://pubmed.ncbi.nlm.nih.gov/24984529/ (accessed July 2022).
10 C. C. Y. Poon and Y. T. Zhang: Conf. Proc. IEEE Eng. Med. Biol. Soc. (2005) 5877. https://doi.org/10.1109/IEMBS.2005.1615827
11 X. R. Ding, Y. T. Zhang, J. Liu, W. X. Dai, and H. K. Tsang: IEEE Trans. Biomed. Eng. **63** (2016) 5. https://doi.org/10.1109/TBME.2015.2480679
12 G. Thambiraj, U. Gandhi, V. Devanand, and U. Mangalanathan: Physiol. Meas. **40** (2019) 7. https://doi.org/10.1088/1361-6579/ab1f17
13 F. S. Cattivelli and H. Garudadri: Proc. 2009 Sixth Int. Workshop on Wearable and Implantable Body Sensor Networks Conf. (2009) 114–119. https://doi.org/10.1109/BSN.2009.35
14 B. Zhang, Z. Wei, J. Ren, Y. Cheng, and Z. Zheng: IEEE Access **6** (2018) 21758. https://doi.org/10.1109/ACCESS.2017.2787980
15 Y. Y. Hsieh, C. D. Wu, S. S. Lu, and Y. Tsao: 2016 IEEE Biomedical Circuits and Systems Conf. (BioCAS) (2016) 604. https://doi.org/10.1109/BioCAS.2016.7833867
16 S. Lee and J. H. Chang: IEEE Trans. Ind. Informat. **13** (2017) 461. https://doi.org/10.1109/TII.2016.2612640
17 E. O'Brien, J. Petrie, W. Littler, M. D. Swiet, P. L. Padfield, D. G. Altmanu, M. Bland, G, A. Coats, and N. Atkins: J. Hypertens. **11** (1993) 677. https://doi.org/10.1097/00004872-199306000-00013
18 F. Pan, P. He, F. Chen, J. Zhang, H. Wang, and D. Zheng: Int. J. Med. Informat. **128** (2019) 71. https://doi.org/10.1016/j.ijmedinf.2019.04.023
19 L. Priyadarshini and L. Shrinivasan: 2020 Int. Conf. Communication and Signal Processing (ICCSP 2020) 1486–1489. https://doi.org/10.1016/j.ijmedinf.2019.04.023
20 J. S. R. Jang: IEEE Trans. Syst. Man Cybern. **23** (1993) 665. https://doi.org/10.1109/21.256541
21 O. Terrada, B. Cherradi, A. Raihani, and O. Bouattane: 2018 Int. Conf. Electronics, Control, Optimization and Computer Science (2018) 1–6. https://doi.org/10.1109/ICECOCS.2018.8610649
22 T. L. Le: IEEE Access **7** (2019) 20967. https://doi.org/10.1109/ACCESS.2019.2895636
23 G. Thambiraj, U. Gandhi, U. Mangalanathan, V. J. M. Jose, and M. Anand: Biomed. Signal Process. Control **60** (2020) 101942. https://doi.org/10.1016/j.bspc.2020.101942
24 Y. Kurylyak, F. Lamonaca, and D. Grimaldi: 2013 IEEE Int. Instrumentation and Measurement Technology Conf. (2013) 280–283. https://doi.org/10.1109/I2MTC.2013.6555424
25 N. Talpur, M. N. M. Salleh, and K. Hussain: Proc. IOP Conf. Ser. Mater. Sci. Eng. **226** (2017) 1. https://doi.org/10.1088/1757-899X/226/1/012103
26 A. L. Goldberger, L. A. N. Amaral, L. Glass, J. M. Hausdorff, P. C. Ivanov, R. G. Mark, J. E. Mietus, G. B. Moody, C. K. Peng, and H. E. Stanley: Circulation **101** (2000) e215. https://doi.org/10.1161/01.CIR.101.23.e215
27 S. M. Lundberg and S. I. Lee: Proc. of the 31st Int. Conf. Neural Information Processing Systems (2017) 4768. https://dl.acm.org/doi/10.5555/3295222.3295230
28 L. Shapley: Contributions to the Theory of Games II, H. Kuhn and A. Tucker, Eds. (Princeton University Press, Princeton, 1953), pp. 307–317. https://doi.org/10.1515/9781400881970-018
29 C. J. Lin, S. Y. Jeng, and M. K. Chen: Appl. Sci. **10** (2020) 2591. https://doi.org/10.3390/app10072591
30 C. Yi, C. Jian, and J. Wenqiang: 14th IEEE Int. Conf. on Electronic Measurement and Instruments (2019) 1656–1663. https://doi.org/10.1109/ICEMI46757.2019.9101774
31 B. Zhang, H. Ren, G. Huang, Y. Cheng, and C. Hu: BMC Bioinformatics **20** (2019) 109. https://doi.org/10.1186/s12859-019-2667-y
32 M. G. Myers, M. Matangi, and J. Kaczorowski: J. Clin. Hypertens. **20** (2018) 1696. https://doi.org/10.1111/jch.13409
33 S. Shimazaki, H. Kawanaka, H. Ishikawa, K. Inoue, and K. Oguri: 41st Annual Int. Conf. of the IEEE Engineering in Medicine and Biology Society (2019) 5042–5045. https://doi.org/10.1109/EMBC.2019.8856706

About the Authors

Cheng-Jian Lin received his B.S. degree in electrical engineering from Ta Tung Institute of Technology, Taipei, Taiwan, R.O.C., in 1986 and his M.S. and Ph.D. degrees in electrical and control engineering from National Chiao Tung University, Taiwan, R.O.C., in 1991 and 1996, respectively. Currently, he is a chair professor of the Computer Science and Information Engineering Department, National Chin-Yi University of Technology, Taichung, Taiwan, R.O.C. and the dean of Intelligence College, National Taichung University of Science and Technology, Taichung, Taiwan, R.O.C. His current research interests are machine learning, pattern recognition, intelligent control, image processing, intelligent manufacturing, and evolutionary robots. (cjlin@ncut.edu.tw)

Mei-Yu Wu received her M.S. and Ph.D. degrees from the Institute of Information Management, National Chiao Tung University, Taiwan, in 1999 and 2005, respectively. Currently, she is an associate professor of the Department of Business Management, National Taichung University of Science and Technology, Taichung, Taiwan, R.O.C. Her research interests include information security management, role-based access control, intelligent agriculture systems, and artificial intelligence applications and management. (mywu@nutc.edu.tw)

Chun-Jung Lin received his MS degree from China Medical University, Taichung, Taiwan, R.O.C., in 2001. He received his Ph.D. degree from the Department of Management of Information System, National Chung Cheng University, Chia-Yi, Taiwan, R.O.C., in 2012. Currently, he is an assistant professor in the Computer Science and Information Engineering Department, National Chin-Yi University of Technology, Taichung, Taiwan, R.O.C. His research interests include database systems, AI applications, healthcare information management, and software engineering. (phdraymond@ncut.edu.tw)

Shih-Lung Shen received his B.S. degree from the Computer Science and Information Engineering Department, National Chin-Yi University of Technology, Taichung, Taiwan, R.O.C., in 2022. Currently, he is a graduate student in the same department. His current research interests are machine learning, pattern recognition, intelligent control, image processing, and FPGA. (r7753pro25@gmail.com)